chemosensors

MDPI

Review

Biosensing Strategies Based on Particle Behavior

Akihisa Miyagawa [1] and Tetsuo Okada [2,3,*]

[1] Department of Chemistry, University of Tsukuba, Tsukuba 305-8577, Japan
[2] Department of Chemistry, Tokyo Institute of Technology, Tokyo 152-8551, Japan
[3] National Institute of Technology (KOSEN), Numazu College, Numazu 410-8501, Japan
* Correspondence: tokada@numazu-ct.ac.jp; Tel.: +81-55-926-5701

Abstract: Micro/nanoparticles are widely used as useful biosensing platforms. Molecular recognition efficiently occurs on their surface, where ligand molecules are accumulated and, in some cases, well organized. The interactions that occur on or in the micro/nanoparticle significantly alter its physicochemical properties. Therefore, highly sensitive detection is possible based on such changes. Usual biosensors convert molecular or biological responses into optical or electrochemical signals. Particle-based biosensing can utilize a variety of other transducing mechanisms, including the changes in the levitation position of particles in physical fields, diffusion behavior, aggregation or dissociation, changes in the surface charge, and changes in size. We review the recent developments in biosensing based on various aspects of particle behavior.

Keywords: nanoparticle; aggregation; surface plasmon; physical force; diffusion; surface charge; DNA; protein

Citation: Miyagawa, A.; Okada, T. Biosensing Strategies Based on Particle Behavior. *Chemosensors* **2023**, *11*, 172. https://doi.org/10.3390/chemosensors11030172

Academic Editor: Vardan Galstyan

Received: 30 January 2023
Revised: 20 February 2023
Accepted: 2 March 2023
Published: 3 March 2023

1. Introduction

Recognition elements and transducers are essential components of biosensors [1–4]. A number of synthetic molecules have been developed that are designed to recognize the target specifically, or at least selectively and, in some cases, have transducer functions. However, they are generally less selective than the molecules found in nature. The concept of supramolecules has been devised to overcome the limitations of such synthetic molecular-based recognition systems. Hayashita et al. reported a boronic acid-modified CyD-based biosensor for glucose [5]. A boronic acid fluorophore is accommodated in the cavity of the boronic acid-modified CyD, forming a supramolecular ligand that selectively complexes with glucose. Fukuhara and Inoue developed an allosteric supramolecule biosensor for dipeptides that was composed of CyD and polythiophene [6]. The dipeptide forms inclusion complexes with two CyD molecules anchored on a polythiophene backbone chain that can induce thiophene twisting and change the chirality of the supramolecule. Other supramolecular systems, which are applicable to biosensing, have also been devised [7–9].

Although the synthesized supramolecular systems allow the flexible design of biosensors for a target molecule, the binding constant and selectivity of these systems are still lower than those of biological systems. Therefore, biomolecules are extensively used as recognition elements because of their high selectivity and stable complexation. Enzymatic reaction, nucleotide hybridization, and antibody–antigen reaction have been often used for biosensing. Enzymes can be used to detect substrates in biological samples; for example, horseradish peroxidase (HRP) can be used to detect H_2O_2 and glucose oxidase (GOx) can be used for glucose detection [10–13]. The use of biological reactions also allows the design of more complex sensing systems.

Sensors must transduce the response of the recognition element to the target into a measurable quantity, such as optical, electric, and electrochemical signals. Optical transducers have been most extensively employed to detect recognition reactions through the changes in the spectral wavelength and spectroscopic signal intensity. All of the principles

of optical measurements, including light absorption [14–16], fluorescence [14–18], and Raman scattering signals [19,20], can be utilized in biosensing transducers. Electrochemical transducers that detect recognition reactions as the changes in the electrochemical potentials and currents are also useful in some cases. Enzyme electrode is one of the simplest biosensors that uses electrochemical transduction. In this approach, targets do not necessarily exhibit direct electrochemical responses but rather are degraded into electroactive substances by enzymatic reactions to ensure sensing selectivity. Because the sensitivity of biosensors relies strongly on the transducing mechanisms, transducer selection is an important factor in the development of efficient biosensing methods.

Advances in micro- and nanotechnology have enabled the preparation of particles of various compositions, including metal, polymer, inorganic, hydrogel, and their composites, with well-defined dimensions ranging from nm to submm. Micro/nanoparticles are highly functional due to their small size, high specific surface area and surface charge, and exhibit unique physicochemical characteristics such as catalytic activity and optical properties. Additional functionalities can be introduced to the particles through a relatively simple pathway [21–23]. Particles with immobilized recognition molecules serve as recognition elements for biosensing and are in some cases more effective than the usual molecular systems. For example, in the lateral flow immunoassay, antibody-modified gold nanoparticles (AuNPs) efficiently recognize antigens and show positive responses in the case of disease [24–26]. The local concentration of the target molecules on the particle surface is higher than that in the bulk solution because the sensor molecules are immobilized in a confined space. Furthermore, molecular orientation is restricted on the particle surface, leading to high efficiency in the reaction with the target [27]. Therefore, sensing reactions tend to proceed more efficiently on the particle surface. Hence, micro/nanoparticles are now indispensable as recognition elements in biosensing systems.

Particles easily aggregate because of their high surface energy. For particles with immobilized functional molecules, aggregation can be induced by surface reactions with the target. Aggregation alters various intrinsic properties of particles, such as size, diffusivity, and optical properties. Therefore, targets can be detected based on the changes in the physicochemical properties and behaviors of the particles caused by aggregation. Microparticles can be directly observed using an optical microscope, and even nanoparticles can be visualized if they are fluorescently labeled. Therefore, particles can serve as efficient transducers for biosensing, enabling the design of sensors that cannot be realized with molecular systems.

In addition, behaviors of micro/nanoparticles in solution can be controlled using external physical fields, such as the magnetic, acoustic, electric, and optical fields [28–31]. Reactions that occur on the surface of or inside the particle alter its physicochemical properties and affect its behaviors in the physical field. In the examples discussed below, the target concentration is converted to length as a measurable quantity in a physical field. When combined with physical fields, the transducing efficiency of particles for biosensing is further enhanced. Thus, micro/nanoparticles not only provide a suitable sensing field for recognition reactions but also act as efficient transducers. In the present review, we discuss biosensing strategies based on various particle behaviors, such as the changes in the levitation position in physical fields, diffusion behavior, particle aggregation or dissociation, changes in the surface charge, and changes in the particle size.

2. Principles of Biosensing Based on Various Particle Behaviors

2.1. Particle Aggregation

Particle aggregation is one of the most common principles of the biosensing [32,33]. Aggregation of noble metal nanoparticles such as AuNPs, silver (AgNPs), and copper nanoparticles is detectable as a change in the color of the solution [34] and has been used for colorimetric sensing. For example, while the suspension of 100 nm AuNPs has a maximum absorption wavelength at 572 nm, aggregation of the AuNPs changes the color of the suspension to blue or purple depending on the number of aggregated AuNPs.

Nanoparticle aggregation can be induced by an appropriate design of the biosensing system. Two different mechanisms of nanoparticle aggregation can be exploited: (1) interparticle crosslinking aggregation, and (2) non-crosslinking aggregation [32,35]. In mechanism (1), the particles are bound to each other through a crosslinking reaction such as DNA hybridization, antibody–antigen reaction, protein–protein reaction, and other specific interactions. Thus, the targets are almost exclusively biomolecules that mediate interparticle reactions, but high selectivity is achieved. By contrast, more diverse targets can induce non-crosslinking particle aggregation, which is caused, for example, by electrostatic interactions. In such cases, detection targets are not limited to biomolecules, but extend to almost all types of chemical substances, including metal ions, small organic molecules, nucleotides, proteins, and even cells.

Although electrostatic interactions usually result in poor selectivity, highly selective non-crosslinking aggregation has also been reported. Maeda et al. showed that a single base difference in DNA is detectable by a color change of the AuNP suspension [36]. AuNPs modified with probe DNA aggregate in the presence of complementary target DNA, turning the AuNP suspension blue. However, if a mismatch is present near the end of the DNA molecule, no color change occurs. Thus, this simple method can distinguish a sequential difference between the target and off-target DNA molecules. Yang et al. proposed an aptamer-based colorimetric detection of dopamine using non-crosslinking AuNP aggregation [37]. Adsorption of dopamine-selective aptamer DNA molecules on AuNPs results in a stable dispersion of AuNPs due to the effect of electrostatic repulsion. When dopamine is added, the aptamer is desorbed from the AuNP surface by the interaction with dopamine, leading to the discoloration of the AuNP suspension due to the aggregation of the AuNPs.

Illumination at an appropriate wavelength excites collective oscillations of conduction electrons in the metal nanoparticles, inducing a strong electromagnetic field on the metal nanoparticle surface, known as localized surface plasmon resonance (LSPR) [38]. When a molecule is found in the region affected by this electromagnetic field near the particle, its Raman scattering is enhanced; this is known as surface-enhanced Raman scattering (SERS). In addition, the superimposition of electromagnetic fields in the gap between the metal surfaces creates hot spots where the SERS intensity is enhanced by a factor of 10^4–10^{11} [39]. Aggregation of metal nanoparticles provides a useful SERS substrate and enables sensitive SERS detection of target molecules.

To efficiently measure SERS and surface enhanced fluorescence signals, novel materials have recently been proposed, named soret colloids [40,41]. This material was synthesized using an adiabatic cooling technique (−18 °C). Soret colloids have a high optical cross section, and the LSPR signal can be controlled by size. The disadvantage was that it took as long as 1–2 h to synthesize colloids of a given size. To overcome this problem, the cryosoret colloids were prepared at lower temperatures (−80, −150, and −196 °C), which made it possible to reduce the preparation time to a few minutes [42]. In addition, nanocarbon florets, which are a spherically isotropic material and have a three-dimensional arrangement of conically graded microcavity, were synthesized [43]. The large pore volume and high surface area of this material improved light confinement and electromagnetic wave localization, enhancing optical signal intensities. Cryosoret and soret colloids, and nanocarbon florets have received attention as novel materials for plasmonics biosensing. Further applications in this field are expected.

Tian et al. developed a SERS platform formed at a liquid–liquid interface for the quantification of trace norepinephirine in the rat brain [44]. AuNPs modified with two different probe molecules, namely, 4-(thiophen-3-ylethynyl)-benzaldehyde and 4-mercaptophenyl boronic acid, self-assemble at the oleic acid/water interface to form a SERS platform. Norepinephirine reacts with the probe molecules to give rigid crosslinked AuNP assemblies with fixed interparticle gaps, resulting in highly reproducible SERS signals. The SERS signal from the C ≡ C group in 4-(thiophen-3-ylethynyl)-benzaldehyde efficiently probes the

target in the silent SERS region and largely eliminates the interreference of any biomolecules present in brain samples. This method enabled the detection of 0.25 nM norepinephirine.

Ren et al. reported label-free detection of native proteins by SERS using iodide-terminated AgNPs that are stably dispersed because of the negative charges of the iodide ions [45]. While proteins are electrostatically attracted to the iodide layer, their direct adsorption on the AgNP surface, which causes structural changes of native proteins, is hindered significantly. This enables reproducible SERS measurements of native proteins. Freezing is also an efficient method for the control of nanoparticle aggregation suitable for SERS measurements. Fukunaga et al. showed that freezing target solutions with AgNPs significantly improves the sensitivity and reproducibility of SERS. When an aqueous solution of a salt or sugar is frozen above the eutectic point, the solutes are concentrated in the freeze-concentrated solution (FCS). The concentration and volume of the FCS obey the phase diagram of the system and can be controlled by the temperature and initial solute concentration [46,47]. The targets are spontaneously concentrated in this process to give high sensitivity. In addition, AgNPs are also concentrated in the FCS together with SERS targets by freezing and aggregate in the FCS. Their aggregation can be controlled by the temperature and initial concentration, and under optimal conditions, the SERS signal intensity was enhanced by a factor of 5000 compared to the nonfreezing conditions.

Changes in the wavelength of the light scattered by metal nanoparticle aggregates have also been used for biosensing. The formation of narrow gaps between nanoparticle aggregates causes strong plasmon coupling and a distinct shift in the LSPR spectrum [48]. Moreover, the scattering intensity depends on the number of aggregated nanoparticles. These changes in the wavelength and intensity of scattered light can be detected using dark-field microscopy. This method is known as the plasmon ruler [49].

Xu et al. reported real-time quantitative detection of microRNA-21 based on the plasmon ruler [50]. Figure 1 schematically represents the plasmon ruler for microRNA sensing. Smaller AuNPs were bound to larger AuNPs (49 nm diameter) by DNA hybridization to form core-satellite nanoparticles. MicroRNA-21 molecules bind the probe DNA molecule anchored on larger AuNPs, dissociating the core-satellite nanoparticles and inducing a blue-shift in the LSPR spectrum. MicroRNA concentration in the nM range was determined based on the statistical analysis of the distribution of the time range in which one strand displacement event occurs.

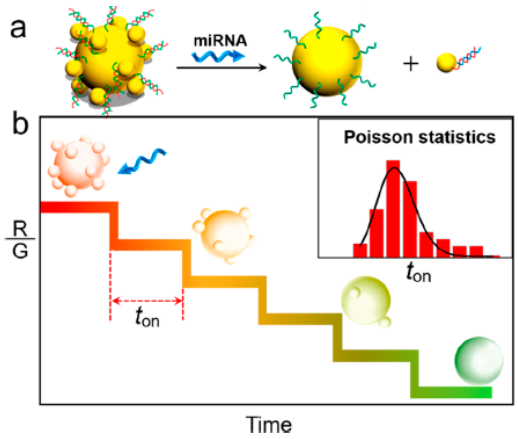

Figure 1. Schematic representation of a plasmon ruler for microRNA sensing. (**a**): Dissociation of smaller AuNPs from the larger AuNP induced by microRNA. (**b**): Detection principle. The dissociation of smaller AuNPs from the larger AuNP shifts the scattering wavelength. Reproduced from Ref. [50] with permission. Copyright 2018 American Chemical Society.

Wei et al. proposed a single-particle assay of poly (ADP-ribose) polymerase-1 (PARP-1) activity using the plasmon ruler [51]. When nicotinamide adenine dinucleotide (NAD^+) reacted with PARP-1 modified on AuNP with the size of 50 nm (Au_{50}), NAD^+ cleaves

to nicotinamide and the ADP-ribose that covalently binds to PARP-1 and polymerize to hyperbranched poly(ADP-ribose) (PAR). When AuNPs with the size of 8 nm (Au_8) were added to this system, a large number of Au_8 entered to the PAR on the Au_{50} because the electrically positive Au_8 adsorbed PAR with abundant negative charges, resulting in a change in the scattering wavelength. This strategy showed high PARP-1 sensitivity with a linear detection range from 0.2 to 10 mU.

2.2. Particle Dissociation from Substrates

Particle dissociation from a flat plate is another useful approach for biosensing. Lammertyn et al. demonstrated a one-step competitive fiber optic SPR bioassay [52] in which AuNPs anchored on the SPR platform through duplex formation with aptamer DNA are dissociated when the target interacts with the aptamer, causing a shift of the SPR wavelength. It was possible to detect the target in the nM-μM range.

Yao et al. proposed a strategy for the detection of tumor-related proteins based on particle dissociation under applied magnetic field [53]. Figure 2 shows the detection principle. DNA (Com)-modified magnetic microparticles were immobilized on the DNA (Cod)-modified substrate through hybridization. Aptamer DNA bound to the rest sequences of Com. When a magnetic field was applied, the magnetic particles were pulled upward. In the absence of proteins, the magnetic particles remained immobilized on the substrate due to the strong interaction with the substrate. The addition of proteins weakened the binding of the particles with the substrate. The particles dissociated from the substrate when the magnetic force exceeded the binding force between Com and Cod. Thus, proteins can be detected based on the magnetic force required for particle dissociation. Because the strength of the interaction between the magnetic particle and the substrate can be controlled by selecting the DNA sequences of Com, Cod, and aptamer, the magnetic force that causes particle dissociation is optimized for the target protein. Therefore, simultaneous detection of multiple proteins was possible in this system.

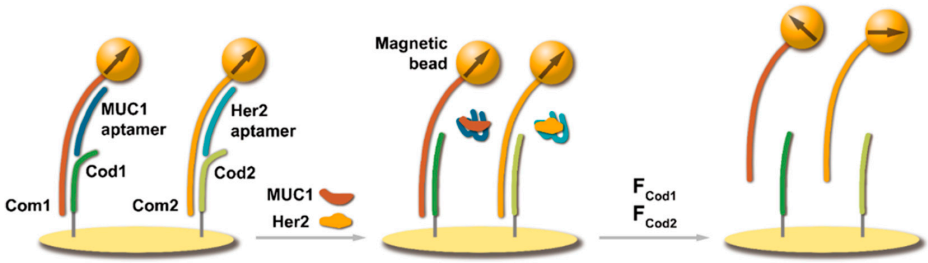

Figure 2. Simultaneous detection of multiplex proteins with magnetic field. Magnetic particles are immobilized on the substrate through DNA hybridization, as shown in the left figure. When target proteins are added, the aptamer interacts with the protein and dissociates, enhancing DNA hybridization between Com and Cod (middle figure). Stronger magnetic forces are required to dissociate magnetic particles from the substrate (right figure). The number of dissociated magnetic particles depends on the concentration of the target protein, allowing detection of multiplex proteins. Reproduced from Ref. [53] with permission. Copyright 2022 American Chemical Society.

Miyagawa et al. proposed a different strategy based on the particle dissociation in a coupled acoustic-gravitational (CAG) field [54,55]. Figure 3 shows the detection principle of this method. DNA-modified microparticles were anchored on the glass plate by DNA hybridization. In the CAG field, the microparticles are simultaneously affected by acoustic radiation (F_{ac}) and sedimentation forces (F_{sed}). When F_{ac}, which is a function of the applied voltage (V) fed to an ultrasound transducer, increases and the total force exceeds the

binding force of duplex DNA (F_{bind}), the particles are dissociated from the glass plate. The threshold voltage required to dissociate the particles is given by [54,55]

$$V = \sqrt{\frac{F_{bind} - A(\rho' - \rho)}{B\left(\frac{5\rho' - 2\rho}{2\rho' + \rho} - \frac{\gamma'}{\gamma}\right)}} \quad (1)$$

$$A = \frac{4}{3}\pi r^3 g \quad (2)$$

$$B = \frac{8\pi^2}{3\lambda} r^3 \alpha \sin\left(\frac{4\pi z}{\lambda}\right) \quad (3)$$

where ρ and γ are the density and compressibility of the medium, respectively (the primes represent the corresponding parameters of the particle), r is the particle radius, g is the gravitational acceleration, λ is the ultrasound wavelength, α is a device-dependent parameter, and z is the distance of the particle from the node of the standing wave. These equations indicate that the threshold voltage depends on the acoustic properties of the particle such as ρ and γ. The density of the microparticles depends on the number of bound AuNPs and can be determined from the threshold voltage. This method enables detection of 2000 DNA molecules per single silica particle.

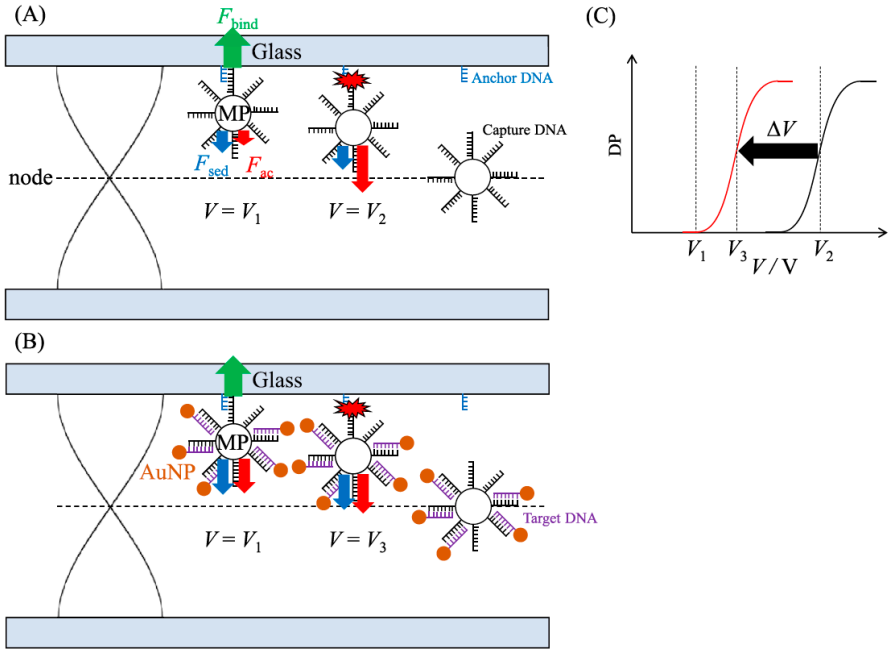

Figure 3. Particle dissociation from the substrate in the CAG field (**A**) without and (**B**) with AuNP binding to the microparticle. (**C**) Relationship between the applied voltage (V) and the dissociation percentage of the microparticles (DP). Reproduced from Ref. [55] with permission. Copyright 2022 Elsevier.

The methods based on particle aggregation and dissociation in the solution are facile and show design flexibility because the probe-modified particle can be easily fabricated in most cases. Furthermore, colorimetry using metal nanoparticles allows the detection of the target molecules not only by absorption spectroscopy but also using the naked eye. However, this method is not sensitive because particles do not aggregate unless a large amount of the target molecule is added. Aggregation of metal nanoparticles also induces high sensitivity in SERS. SERS sensitivity depends on the distance between the nanoparticles in the aggregate, which is generally difficult to control, decreasing the reproducibility of the SERS measurements. Although control of the interparticle gap using the reaction of the target molecules is effective for highly reproducible SERS measurements,

expanding the range of target molecules is the next challenge in the further development of this approach. Versatile designs of highly sensitive sensors are possible utilizing particle dissociation from the substrate. In addition, this approach has another advantage of low sample consumption due to the small number of particles required.

2.3. Levitation of Particles in Physical Fields

External physical fields, including optical, electric, dielectric, magnetic, and acoustic fields, have been used for microparticle manipulation. The physical force acting on a particle is a function of several physical properties, including the particle size, shape, deformation, density, electronic charge, compressibility, permittivity, and magnetic susceptibility. Therefore, microparticle manipulation and separation can be performed according to the specific properties of the particles by selecting an appropriate physical field. Readers interested in this topic can refer to our previous paper reviewing microparticle manipulation in various physical fields [31].

Particle levitation by physical fields is a typical approach for particle manipulation. The use of optical tweezers invented by Ashkin [56] has become a popular technique, and optical tweezers have been utilized in various fundamental and applied scientific fields and have found a number of applications. The difference in the refractive index between the medium and the particle is a key parameter that determines the optical force acting on the particle. Ultrasound levitation, which is another useful approach for particle manipulation, relies on the acoustic radiation force, the effect of which varies as a function of the particle radius, density, and compressibility [57,58]. In addition, magnetic particles can be manipulated and levitated in a magnetic field according to their radius, density, and magnetic susceptibility [59,60]. Thus, different physical forces interact with different particle properties. Therefore, in a well-designed physical field, particles show different behaviors depending on their physical properties, and novel sensing principles can be derived based on particle behavior.

Whiteside et al. proposed a novel technique of particle levitation using a magnetic field, named MagLev [61–65]. Figure 4 shows a representative geometry of MagLev. Diamagnetic microparticles dispersed in the paramagnetic medium are placed between two permanent magnets. In this geometry, magnetic and sedimentation forces act on the particles, and the particles are levitated at the position where these two forces are equal. The levitation height (h) from the bottom of the cell is given by [61–65]

$$h = \frac{(\rho_p - \rho_m) g \mu_0 d^2}{(\chi_p - \chi_m) 4 B_0^2} + \frac{d}{2} \quad (4)$$

where μ_0 is the magnetic permeability of vacuum, d is the distance between the two magnets, χ is the magnetic susceptibility, B_0 is the magnetic strength at the surface of the magnets, and the subscripts p and m represent the particle and the medium, respectively. Equation (4) indicates that h of the diamagnetic particle depends on ρ_p and χ_p. Based on the principle of MagLev, particle separation was performed [66]. This principle indicates that the change in the physical property of the particle causes a shift in the levitation height. Therefore, if the particle properties change due to the reaction inside the particle or on the particle surface, h will change, suggesting that the progress of the reaction can be evaluated from the change in h. Whitesides et al. applied MagLev to the evaluation of the kinetics of free-radical polymerization [63]. In this study, the time evolution of h of the microdroplet was monitored during the polymerization that changes the microdroplet density.

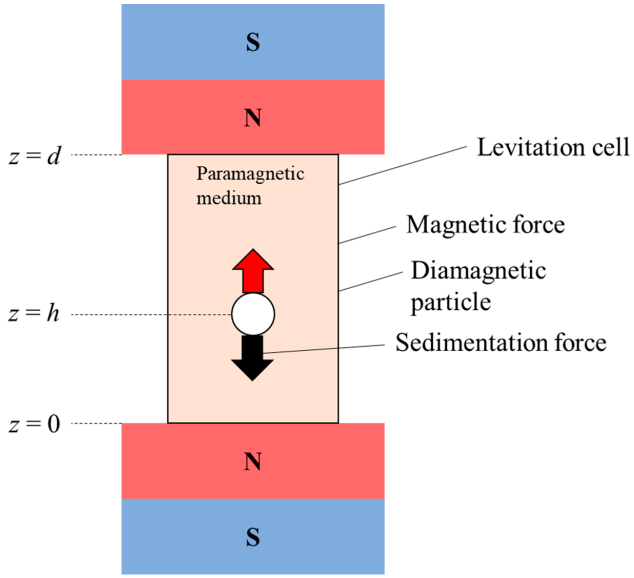

Figure 4. Representative setup of MagLev.

MagLev was further applied to biosensing. Özefe and Yildiz reported a Hepatitis C (HCV) detection assay using MagLev [67]. Changes in the microparticle density due to the interaction between the HCV NS3 protein and the anti-HCV NS3 antibody immobilized on the microparticle surface were detected by the shift of its levitation position. The detection limit was 50 μg mL^{-1} of the HCV NS3 protein. Tekin et al. proposed a magnetic-susceptibility-based protein detection scheme using MagLev (Figure 5) [68]. The target proteins were sandwiched between two particles, namely, the antibody-modified microparticle and the magnetic nanoparticle. The levitation height was altered by a change in the susceptibility of the microparticle–protein–nanoparticle complex. This approach enabled the detection of 10 ng mL^{-1} bovine serum albumin (BSA) and 1.5 ng mL^{-1} immunogloblin G. The resolution of the volume magnetic susceptibility in this method was as high as 4.2×10^{-8} μm^{-1}. Ghiran et al. detected membrane-bound and soluble antigens based on the MagLev principle [69]. Microparticles with different densities (1.05 and 1.2 g cm^{-3}) were modified by capture- and detection-antibodies, respectively. These two particles bound to each other in the presence of antigens to form a particle complex with an intermediate density so that the levitation position of the particle complex was distinguished from those of the unreacted microparticles. This enabled the successful detection of various antigens.

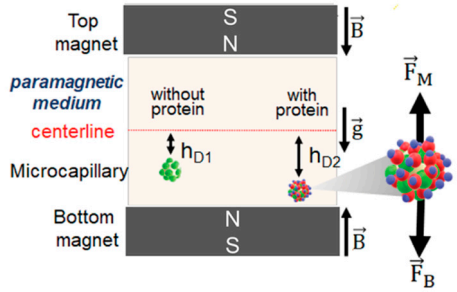

Figure 5. Schematic representation of MagLev for detection of protein based on the magnetic susceptibility change. Reproduced from Ref. [68] with permission. Copyright 2020 American Chemical Society.

We developed biosensing methods based on the acoustic levitation of microparticles [66–70]. When an acoustic standing wave is vertically generated, the CAG field is formed. In this field, the microparticles are subjected to the combined force of F_{ac} and F_{sed}

and are levitated at the position where these two forces are balanced. This position (z) is given by the following equations [70–74].

$$z = \frac{\lambda}{4\pi} \sin^{-1}\left\{ \frac{(\rho_m - \rho_p) g \lambda}{A \alpha V^2 2\pi} \right\} \quad (5)$$

$$A = \frac{5\rho_p - 2\rho_m}{2\rho_p + \rho_m} - \frac{\gamma_p}{\gamma_m} \quad (6)$$

The parameters in these equations were already defined for Equations (1)–(3). Equations (5) and (6) indicate that z depends on ρ_p and γ_p but is independent of the particle size. If the reaction on the particle leads to a density change, it can be detected as a change in z.

This concept enabled zmol detection of the avidin–biotin reaction (Figure 6) [74,75]. Avidin-modified polymer microparticles reacted with biotin-modified AuNPs. Because the density of AuNPs is much larger than that of the polymer, the binding of AuNPs increased the density of the microparticle and decreased its levitation position. This concept was also extended to the biosensing of nucleic acids [72,73]. Microparticles were bound to AuNPs by sandwich hybridization with target DNA. The interparticle sandwich DNA-hybridization induces an increase in the density of the microparticles. Several thousand DNA molecules were successfully detected. In addition, single polymorphism of the KRAS gene was detected by controlling the length of the complementary probe DNA molecules immobilized on the particles.

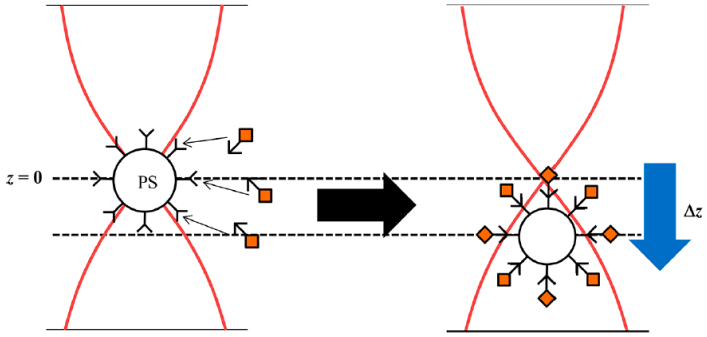

Figure 6. Schematic representation of the acoustic levitation for detection of the avidin–biotin reaction based on the density change. Reproduced from Ref. [74] with permission. Copyright 2018 American Chemical Society.

By using microparticles with different diameters, multiple targets are simultaneously detected with the CAG. The usefulness of this concept was demonstrated in microRNA sensing [72]. In the CAG field, particles with different sizes cannot be distinguished as shown by Equation (5). However, the density of the smaller particles becomes larger than that of the larger particles when the same number of AuNPs are bound. Based on this principle, miR-21 and miR-122, which are related to hepatocellular carcinoma, were simultaneously detected at the zmol level. We also proposed aptamer-based biosensing of several physiologically active substances using the CAG field [71]. AuNP-bound microparticles were prepared by sandwich hybridization using aptamer DNA designed for a specific target. When a target is added to the AuNP-bound microparticles, the aptamer DNA interacts with the target and dissociates AuNPs from the microparticle. Thus, the levitation position of the microparticle changes due to the decrease in the density. For this method, detectability depends strongly on the binding constants of the aptamer-target complexes. The detection limits for ATP, dopamine, and ampicillin were 9.8 nM, 17 nM, and 160 pM, respectively.

A key feature of the detection schemes based on the levitation position in a physical field is that the reactions inside of or on the particle affect the levitation positions, enabling quantifi-

cation. The reaction of trace reactants can also be detected as differences in the microparticle behavior that can be observed under a microscope. In addition, highly sensitive detection is possible because a single particle is levitated in magnetic or acoustic fields. However, sensing based on particle levitation has an intrinsic drawback in that its application is limited to micrometer-sized particles because both magnetic and acoustic forces are proportional to the particle volume and weaken with decreasing particle size. In addition, both magnetic and acoustic fields have inherent disadvantages in the design of biosensing systems. In MagLev, ferrofluids such as $MnCl_2$ and $GdCl_3$ solutions with high concentrations (on the order of several M) should be used as the medium. Unfortunately, high salt concentrations give rise to various unwelcome phenomena, such as protein denaturation and destabilization of the DNA duplex. This restricts the application of MagLev to biosensing. On the other hand, acoustic measurements in the CAG field require a refined cell made of homogeneous materials with controlled thickness. While acoustic levitation can be performed in any observation cell, the precise levitation position is difficult to determine without the refined cell. This restricts the application of the CAG field to biosensing.

2.4. Change in the Particle Size

The physical and chemical properties of metal and mineral nanoparticles depend on their size [76,77]. Therefore, particle size is an important factor in applications. As described in Section 2.1, nanoparticle suspensions exhibit specific colors because of LSPR depending on their size due to the changes in the absorption and emission wavelengths. Although the size of the microparticles can be directly measured, it is difficult to accurately measure minute size changes caused by biochemical reactions. This difficulty is even more acute for nanoparticles. Therefore, an appropriate strategy is required to evaluate the changes in the particle size as discussed below.

Hydrogels have been used for size-based biosensing because their volume changes depending on various factors, such as the crosslinking degree of their constituent polymers and their water content [77–80]. Furthermore, hydrogels are suitable for use in diagnostic applications because of their solution-like environments, ease of chemical modification, and low susceptibility to contaminants in biological fluids. Park et al. reported a hydrogel-based glucose biosensor using dual-mode detection of fluorescence quenching and size reduction [81]. Poly(acrylic acid) gels immobilized with carbon dots, glucose oxidase (GOx), and horseradish peroxidase (HRP) were prepared. The hydrogel particles emitted fluorescence from carbon dots. In the presence of glucose, bienzymatic reactions by GOx and HRP produced gluconic acid and hydroxyl radicals that consumed water in the hydrogel and reduced the particle size. In addition, the produced hydroxyl radicals quenched the fluorescence from the hydrogels. Ravaine et al. designed glucose-responsive hydrogels composed of *N*-alkylacrylamide derivatives and phenylboronic acid (PBA) [82]. Hydrogel swelling was controlled by varying the ratio of PBA to the total polymer. Fructose, which forms a 1:1 complex with PBA, promoted hydrogel swelling, while glucose caused hydrogel shrinking by reacting with two PBA molecules. Shah et al. developed a biosensing platform using a hydrogel composed of PEG-cross-linked polyacrylamide functionalized with 3-(acrylamido)phenylboronic acid (APBA) [83]. Optical coherence tomography enabled 3D observations with high spatial and temporal resolutions. The reaction of glucose and APBA, which caused hydrogel shrinking, was dynamically detected.

Ekinci et al. proposed a different sensing mechanism utilizing the changes in the particle size. Nanoparticles of different diameters were used for virus detection [84]. In a conical nanofluidic channel with a tapered outflow side, antibody-modified nanoparticles with various diameters were trapped at the positions where the particle diameter matched the nanochannel size. Virus-bound nanoparticles modified by fluorescently labeled antibodies were detected. In particular, the SARS-CoV-2 and influenza A viruses were detected at the nM level.

Chen et al. developed microchannel resistance biosensing based on the Coulter principle, as shown in Figure 7 [85]. When microparticles with sizes comparable to the channel

diameter are introduced into the channel, the DC current is disrupted by the increased resistance caused by the passage of the particles. The resistance of the microchannel (R') during the passage of the particles is given by [85]

$$R' = N\frac{2\arctan\left(d/2/\sqrt{(S/\pi)-(d/2)^2}\right)}{\sigma\pi\sqrt{(S/\pi)-(d/2)^2}} + \frac{l-Nd}{\sigma S} \quad (7)$$

where N is the number of the microparticles in the channel, d is the particle diameter, σ is the electric conductivity of the electrolyte solution, S is the cross-sectional area of the channel, and l is the length of the channel. This equation indicates that R' depends on d and N. Target molecules mediated the sandwich reaction between the microparticles and magnetic beads, increasing the particle size. This event was detected by an increase in the resistance of the channel. The detection limits of procalcitonin, chlorpyrifos, and *L. monocytogenes* were 1.58 pg mL^{-1}, 1.16 pg mL^{-1}, and 47.89 cfu mL^{-1}, respectively.

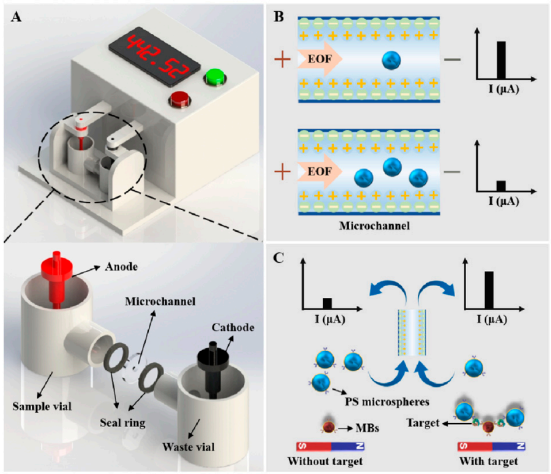

Figure 7. Biosensing principle based on the measurements of the microchannel resistance. (**A**) Biosensing device. (**B**) Dependence of the current signals on the number of the particles in the channel. (**C**) Variation of the current signals with particle size. Reproduced from Ref. [85] with permission. Copyright 2021 American Chemical Society.

2.5. Particle Motion

Brownian motion is due to the self-driven and random colloidal movements of micro/nanoparticles. Based on the Stokes–Einstein equation, the diffusion coefficient of the translational Brownian motion (D_t) of a particle is given by the following equation [86].

$$D_t = \frac{k_B T}{6\pi\eta r} \quad (8)$$

where k_B is the Boltzmann constant, T is the absolute temperature, η is the medium viscosity, and r is the particle radius. Thus, particle diffusion is a function of the particle radius and the viscosity of the medium. Therefore, translational diffusometry can be used to evaluate the microenvironment viscosity.

Particle behavior is difficult to control because of three-dimensional random Brownian motion, and, therefore, physical fields are often used to prevent particle motion. However, some researchers have proposed biosensing schemes that utilize translational Brownian motion itself. Wereley et al. applied translational particle diffusometry to DNA detection [87]. The increase in the viscosity due to the DNA amplification of the specific genes from *S. aureus* and *K. pnuemoniae* was measured as the changes in the particle diffusion observed by fluorescence microscopy. Kinzer–Ursem et al. determined the association

constant of the avidin–biotin binding that occurs on the nanoparticle surface based on the changes in the particle diffusion coefficient [88]. When avidin-modified nanoparticles (20 nm) react with biotin-modified nanoparticles (200 nm), larger particles are formed. As seen from Equation (8), this interparticle reaction resulted in a decrease in D_t. In this study, the interparticle avidin–biotin reaction was dynamically observed in a microfluidic channel. The particle diffusion coefficient was measured at some points along the microchannel axis. The binding rate constant was determined to be 1.74×10^7 M^{-1} s^{-1}.

Chuang et al. reported novel pathogen detection using rotational diffusometry [89]. According to the Stokes–Einstein–Debye relation, the rotational diffusion coefficient (D_r) is written as [89,90]

$$D_r = \frac{k_B T}{\pi \mu {d_p}^3} \quad (9)$$

where d_p is the particle diameter. This equation indicates that D_r depends on the solvent viscosity and particle size. Thus, DNA amplification of a specific gene increased viscosity, resulting in a decrease in D_r. This scheme was applied to the detection of the *Escherishia coli* pathogen. Janus particles, for which one half of the particle is modified with a fluorescence dye and the other half is coated with a thin gold film, were used as rotation probes. The detection limit of this method was 50 pg μL^{-1} of *E. coli* genomic DNA with a measurement time of 30 s and a sample volume of 2 µL. They also proposed another mechanism of rotational diffusometry [90]. Equations (8) and (9) indicate that particle size has a greater effect on the rotational diffusion of the particle than on its translational diffusion because D_r is a function of ${d_p}^3$ whereas D_t is a function of d_p. The Janus microparticle half-functionalized with antibodies bound to antibody-modified nanoparticles in the presence of the tumor necrosis factor-α cytokine target. This interparticle reaction caused an increase in the particle size that was observed as a change in D_r. The detection limit was 1 pg mL^{-1}.

The temporal changes of the motion of the particles tethered to the substrate have also been proposed as a mechanism for biosensing. Prins et al. devised the concept schematically shown in Figure 8 [91,92]. Microparticles functionalized with the target analogue were tethered on the substrate via a double-strand DNA chain with 50 base pairs. The substrate surface was modified with detection molecules. The microparticles bound to the substrate surface by the interaction between the detection molecule and the target analogue. In the presence of the targets, the detection molecules on the substrate surface interacted with the target molecules, dissociating the binding between the microparticle and the substrate. This event was optically detected via the Brownian motion of the microparticles. The binding events of short DNA and creatinine were successfully monitored. Dongen et al. demonstrated a multiplex hairpin-DNA sensor based on the fluctuation in the plasmonic signal intensity [93]. The AuNPs were tethered on the gold film substrate using hairpin DNA that adopts the folded structure in the absence of the target. The plasmonic signal intensity, which depends on the distance between the AuNPs and the gold substrate, varies due to the Brownian motion of the AuNPs. In the folded state of the hairpin DNA, the fluctuation of the signal intensity is small because of the small gap between the AuNPs and the substrate. By contrast, when the target DNA interacted with the hairpin DNA, the gap increased, and the signal fluctuated strongly. In addition, the plasmonic signal fluctuation varied with the length of the unbound sequence in the hairpin DNA. Based on this variation, multiple target DNA molecules with different lengths were successfully detected.

The translational and rotational diffusion of the particle can be evaluated within several minutes because particle trajectories can be measured by high-speed microscopy. Therefore, diffusometry is suitable for biomolecule detection required for early disease diagnosis. To enhance sensitivity, the use of nanoparticles is desirable. However, microparticles are required due to the use of an optical microscope. Diffusion of the nanoparticles has not been exploited in practical use in biosensing because it requires a complex experimental setup.

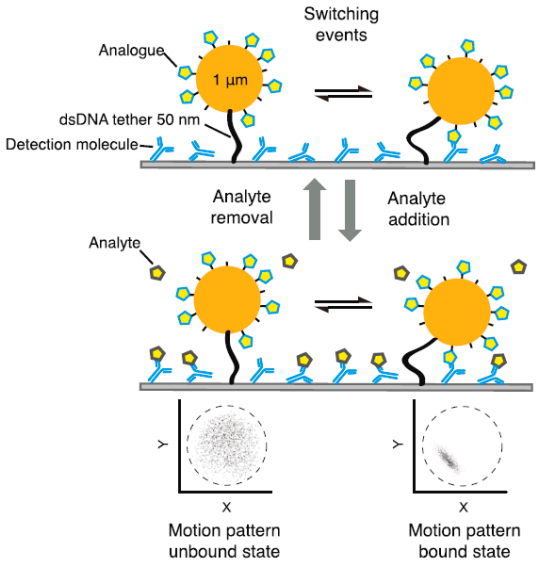

Figure 8. Particle motion on the substrate. Microparticles are tethered on the substrate using DNA duplex. When analogues immobilized on the microparticle interact with the detection molecule on the substrate, particle motion is restricted. In the presence of the analyte, the motion of the microparticle is no longer restricted because the detection molecules are blocked by the analytes. Reproduced from Ref. [92] with permission. © 2020. This work is licensed under a CC BY 4.0 license.

2.6. Change in the Surface Charge

Surface charges are present at all interfaces, including solid–air, solid–liquid, liquid–liquid interfaces, and play an important role in chemical, industrial, and biological processes. Under an applied electric field, the materials comprising the interface are subjected to electric forces corresponding to their interfacial charges. A fluid in contact with a large mass of solid moves to generate an electroosomotic flow. By contrast, micro/nanoparticles dispersed in a liquid migrate by electrophoresis. Particles with different surface charges can be separated by the difference in the electrophoretic mobility in an electric field [94,95]. Therefore, the behavior of particles in an electric field reflects their surface charge. Biosensing based on the changes in the surface charge has been performed using various detection techniques.

Tao et al. evaluated the kinetics of ligand–protein interactions using coupling plasmon imaging in an oscillated electric field (Figure 9) [96,97]. When light is irradiated from the back of a glass slide coated with a thin gold layer, evanescent (plasmonic) waves are generated on the gold surface [98,99]. Plasmonic waves are scattered by particles on the gold surface, enabling measurement of plasmonic images with high contrast. The exponential decrease in the plasmonic intensity with increasing distance from the gold surface enabled the measurement of the distance between the particle and surface with a precision on the order of nm. When alternating voltage was applied to protein-modified silica particles tethered on a gold-coated glass plate, the particles oscillated with an amplitude corresponding to their surface charge densities. The binding of ligands to the protein on the particle changed the oscillation amplitude. The kinetics of ligand–protein binding (BSA-antiBSA and membrane proteins with small molecules) was evaluated.

Chen et al. demonstrated electrochemiluminescence biosensing of hyaluronidase (HAse) exploiting electrostatic interactions [100]. Hyaluronic acid-coated amino-modified silica particles doped with ruthenium bipyridine ($Ru@SiO_2$-NH_2@HA NPs) were synthesized as electrochemiluminescence indicators. No electrochemiluminescence signals were obtained due to the electrostatic repulsion between the negatively charged particle and the indium tin oxide electrode with the same sign of the charge. HAse decomposed hyaluronic acids to give amino groups on the silica particle, resulting in positive charges on the particles. Electrochemiluminescence was observed due to electrostatic adsorption of positively charged particles on the electrode. The detection limit was 0.37 U mL^{-1}.

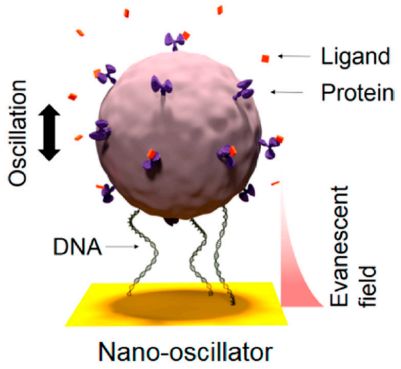

Figure 9. Schematic representation of particle oscillation anchored on a gold substrate by alternating voltage. The particle was tethered by DNA duplexes. When AC voltage was applied, the particle was oscillated according to the surface charge of the particle. The distance from the substrate was measured using a plasmon imaging technique. Reproduced from Ref. [96] with permission. Copyright 2019 American Chemical Society.

The zeta potential (ζ) is a physical parameter that depends on the surface charge density (σ_d). Assuming that ζ is equal to the surface potential, the Gouy–Chapman–Stern model for the electrical double layer yields the following equation [101,102].

$$\sigma_d = \sqrt{8RT\varepsilon_0\varepsilon c}\sin h\left(\frac{zF\zeta}{2RT}\right) \quad (10)$$

where R is the gas constant, ε_0 is the permittivity in vacuum, ε is the relative permittivity of the medium, c is the concentration of a 1:1 salt, z is the charge of the ions, and F is the Faraday constant. Equation (10) indicates that the binding of proteins to the particle changes its surface charge density and, in turn, its zeta potential. Miyagawa et al. proposed direct quantification of proteins from the change in the zeta potential of carboxy-functionalized microparticles [103]. Equation (10) explains the pH dependence of the protein-modified particle well by considering the dissociation of the acidic and basic amino acids contained in the proteins. The detection limits of BSA, myoglobin, and lysozyme were 1.17×10^4, 1.22×10^4, and 1.20×10^4 per microparticle, respectively.

In solution, all molecules exist in either a charged or uncharged state. The detection principle based on the changes in the surface charge of the particles can in principle be applied to any system, because the surface charge is affected by the environment. In addition, this concept is effective not only for microparticles but also for nanoparticles because electric force can be applied irrespective of the size of the material. However, surface charge depends strongly on the surrounding environment, including the ionic strength and the concentrations of other coexisting substances. Nonspecific adsorption and electrostatic interaction of off-target biomolecules can affect the surface charge of probe particles, hindering the application of this mechanism to biological samples containing various contaminants.

3. Conclusions

Particle-based biosensors reviewed in this paper are summarized in Table 1. We have discussed biosensing strategies based on the behavior of micro- and nanoparticles. Particles can function not only as a part of sensing elements but also as transducers. One of the important features of particles in biosensing is that they can be easily functionalized by immobilizing various molecules on the surface to serve as sensing elements that recognize specific targets. Because of the large surface area relative to the volume of micro/nanoparticles, target recognition occurring on their surface significantly changes their physicochemical properties, resulting in high sensitivity. In addition, particles provide specific transducing mechanisms that are different from those of the usual optical and

electrochemical transducers. Here, we have reviewed various particle behaviors, such as aggregation, SERS, dissociation from the substrate, levitation in a physical field, particle motion, plasmon imaging, electrochemiluminescence, zeta potential, size, and electric current modulation. Most of these are unique to particle-based sensing and, therefore, cannot be achieved in molecule-based sensing. Composite materials that exhibit interesting physical properties have been studied. Nanoparticles fabricated with such materials have high potential for the design of biosensors with novel transducer capability [104–107].

Table 1. Summary of biosensors based on the particle behavior.

Particle Behavior	Particle Type	Detection Method	Target	Ref
Aggregation	AuNP	SERS	Norepinephrine	[44]
	AuNP	SERS	Lysozyme, avidin, BSA, cytochrome *c*, and hemoglobin	[45]
	AgNP	SERS	DNA bases	[46,47]
Dissociation	AuNP	LSPR wavelength	MicroRNA-21	[50]
	AuNP	LSPR wavelength	Polymerase activity	[51]
	AuNP	SPR wavelength	ATP, thrombin, and single strand DNA (ssDNA)	[52]
	Magnetic microparticle	Optical observation	Mucin-1 glycoprotein and human epidermal growth factor receptor	[53]
	Silica and polystyrene (PS) microparticles and AuNPs	Optical observation	Double-strand DNA (dsDNA)	[54,55]
Levitation	PS microparticle	Optical observation	HCV	[67]
	PS microparticle and magnetic nanoparticle	Optical and fluorescence observation	BSA and mouse immunoglobulin G	[68]
	Polymethylmethacrylate (PMMA) microparticle	Optical observation	T-cell antigen CD3, eosinophil antigen Siglec-8, red blood cell antigens CD35 and RhD, red blood cell-bound Ep-stein-Barr viral particle, and soluble IL-6	[69]
	PS and PMMA microparticles and AuNP	Optical observation	Avidin–biotin complex, ssDNA, dsDNA, microRNA-21 and microRNA-122, ATP, dopamine, and ampicillin	[72–75]
Size	Poly(acrylic acid) hydrogel	Optical observation and fluorescence intensity	Glucose	[81]
	Poly(aspartic acid) hydrogel	Optical observation	Glucose	[82]
	Poly(acrylamide) hydrogel	Optical coherent tomography	Glucose	[83]
Motion	Magnetic nanoparticle	Fluorescence observation	SARS-CoV-2 and influenza A	[84]
	PS and magnetic microparticle	Electric resistance	Procalcitonin, chlorpyrifos, and *L. monocytogenes*	[85]
	PS nanoparticle	Fluorescence observation	*S. aureus* and *K. Pneumoniae*	[86]
	Polymer nanoparticle	Fluorescence observation	Avidin–biotin complex	[88]
	Janus microparticle and PS nanoparticle	Fluorescence observation	DNA and tumor necrosis factor-α cytokine target	[89,90]
	Magnetic microparticle	Optical observation	ssDNA and creatinine	[91,92]
Surface charge	AuNP	Plasmon imaging	ssDNA	[93]
	Silica microparticle	Plasmon imaging	BSA, nanodisc encapsulated membrane protein KcsA-Kv1.3	[96,97]
	Silica nanoparticle	Electrochemiluminescence	Hyaluronidase	[100]
	PS microparticle	Zeta potential	BSA, myoglobin, Lysozyme	[103]

Hence, particles facilitate the design of biosensors with regard to both recognition elements and transducers. It is expected that researchers will continue to propose novel ideas that take advantage of the unique properties of particles. We believe that particle-based biosensing will become the gold standard in a wide range of analytical chemistry applications and will contribute to advances in related disciplines.

Author Contributions: Conceptualization, A.M. and T.O.; writing—original draft preparation, A.M.; writing—review and editing, T.O.; supervision, T.O. All authors have read and agreed to the published version of the manuscript.

Funding: The authors received no financial support for this study.

Institutional Review Board Statement: Not applicable.

Informed Consent Statement: Not applicable.

Data Availability Statement: Not applicable.

Conflicts of Interest: The authors declare no conflict of interest.

References

1. Zhao, Y.; Tong, R.-J.; Xia, F.; Peng, Y. Current status of optical fiber biosensor based on surface plasmon resonance. *Biosens. Bioelectron.* **2019**, *142*, 111505. [CrossRef] [PubMed]
2. Low, S.S.; Chen, Z.; Li, Y.; Lu, Y.; Liu, Q. Design principle in biosensing: Critical analysis based on graphitic carbon nitride (G-C_3N_4) photoelectrochemical biosensor. *TrAC Trends Anal. Chem.* **2021**, *145*, 116454. [CrossRef]
3. Wang, X.; Lu, X.; Chen, J. Development of biosensor technologies for analysis of environmental contaminants. *Trends Environ. Anal. Chem.* **2014**, *2*, 25–32. [CrossRef]
4. Guo, X. Surface plasmon resonance based biosensor technique: A review. *J. Biophoton.* **2012**, *5*, 483–501. [CrossRef]
5. Kumai, M.; Kozuka, S.; Hashimoto, T.; Suzuki, I.; Hayashita, T. Glucose Recognition by a Supramolecular Complex of Boronic. *Anal. Sci.* **2012**, *28*, 121–126. [CrossRef]
6. Fukuhara, G.; Inoue, Y. Peptide chirality sensing by a cyclodextrin-polythiophene conjugate. *Chem. Eur. J.* **2012**, *18*, 11459–11464. [CrossRef]
7. Ma, D.; Zhang, L.-M. Novel biosensing platform based on self-assembled supramolecular hydrogel. *Mater. Sci. Eng.* **2013**, *33*, 2632–2638. [CrossRef]
8. Fukuhara, G. Smart Polymer chemosensors: Signal-amplification systems with allosterism. *Polym. J.* **2021**, *53*, 1325–1334. [CrossRef]
9. Barrow, S.J.; Kasera, S.; Rowlannd, M.J.; del Barrio, J.; Scherman, O.A. Cucurbituril-Based Molecular Recognition. *Chem. Rev.* **2015**, *115*, 12320–12406. [CrossRef]
10. Berchmans, S.; Venkatesan, M.; Vusa, C.S.R.; Arumugam, P. PAMAM Dendrimer Modified Reduced Graphene Oxide Postfunctionalized by Horseradish Peroxidase for Biosensing H_2O_2. *Methods Enzymol.* **2018**, *609*, 143–170. [CrossRef]
11. Liu, X.; Luo, L.; Ding, Y.; Xu, Y.; Li, F. Hydrogen peroxide biosensor based on the immobilization of horseradish peroxidase on γ-Al_2O_3 nanoparticles/chitosan film-modified electrode. *J. Solid State Electrochem.* **2011**, *15*, 447–453. [CrossRef]
12. Rasheed, T.; Hassan, A.A.; Kausar, F.; Sher, F.; Bilal, M.; Iqbal, H.M.N. Carbon nanotubes assisted analytical detection—Sensing/delivery cues for environmental and biomedical monitoring. *TrAC Trends Anal. Chem.* **2020**, *132*, 116066. [CrossRef]
13. Fu, L.-H.; Qi, C.; Lin, J.; Huang, P. Catalytic chemistry of glucose oxidase in cancer diagnosis and treatment. *Chem. Soc. Rev.* **2018**, *47*, 6454–6472. [CrossRef] [PubMed]
14. Dongare, P.R.; Gore, A.H. Recent Advances in Colorimetric and Fluorescent Chemosensors for Ionic Species: Design, Principle and Optical Signalling Mechanism. *ChemistrySelect* **2021**, *6*, 5657–5669. [CrossRef]
15. Fukuhara, G. Allosteric signal-amplification sensing with polymer-based supramolecular hosts. *J. Incl. Phenom. Macrocycl. Chem.* **2019**, *93*, 127–143. [CrossRef]
16. Fukuhara, G. Analytical supramolecular chemistry: Colorimetric and fluorimetric chemosensors. *J. Photochem. Photobiol. C* **2020**, *42*, 100340. [CrossRef]
17. Cao, D.; Zhu, L.; Liu, Z.; Lin, W. Through bond energy transfer (TBET)-based fluorescent chemosensors. *J. Photochem. Photobiol. C* **2020**, *44*, 100371. [CrossRef]
18. Móczár, I.; Huszthy, P. Optically active crown ether-based fluorescent sensor molecules: A mini-review. *Chirality* **2019**, *31*, 97–109. [CrossRef]
19. Ji, W.; Li, L.; Zhang, Y.; Wang, X.; Ozaki, Y. Recent advances in surface-enhanced Raman scattering-based sensors for the detection of inorganic ions: Sensing mechanism and beyond. *J. Raman Spectrosc.* **2021**, *52*, 468–481. [CrossRef]
20. Lin, S.; Cheng, Z.; Li, Q.; Wang, R.; Yu, F. Toward Sensitive and Reliable Surface-Enhanced Raman Scattering Imaging: From Rational Design to Biomedical Applications. *ACS Sens.* **2021**, *6*, 3912–3932. [CrossRef]
21. Sun, X.-T.; Liu, M.; Xu, Z.-R. Microfluidic fabrication of multifunctional particles and their analytical applications. *Talanta* **2014**, *121*, 163–177. [CrossRef]
22. Jones, O.G.; McClements, D.J. Functional Biopolymer Particles: Design, Fabrication, and Applications. *Compr. Rev. Food Sci. Food Saf.* **2010**, *9*, 374–397. [CrossRef]
23. Tardy, B.L.; Mattos, B.D.; Otoni, C.G.; Beaumont, M.; Majoinen, J.; Kämäräinen, T.; Rojas, O.J. Deconstruction and Reassembly of Renewable Polymers and Biocolloids into Next Generation Structured Materials. *Chem. Rev.* **2021**, *121*, 14088–14188. [CrossRef]

24. Shan, S.; Lai, W.; Xiong, Y.; Wei, H.; Xu, H. Novel strategies to enhance lateral flow immunoassay sensitivity for detecting foodborne pathogens. *J. Agric. Food Chem.* **2015**, *63*, 745–753. [CrossRef] [PubMed]
25. Chen, A.; Yang, S. Replacing antibodies with aptamers in lateral flow immunoassay. *Biosens. Bioelectron.* **2015**, *71*, 230–242. [CrossRef]
26. Xing, K.-Y.; Shan, S.; Liu, D.-F.; Lai, W.-H. Recent advances of lateral flow immunoassay for mycotoxins detection. *TrAC Trends Anal. Chem.* **2020**, *133*, 116087. [CrossRef]
27. Fong, L.-K.; Wang, Z.; Schatz, G.C.; Luijten, E.; Mirkin, C.A. The Role of Structural Enthalpy in Spherical Nucleic Acid Hybridization. *J. Am. Chem. Soc.* **2018**, *140*, 6226–6230. [CrossRef]
28. Semenova, M. Protein–polysaccharide associative interactions in the design of tailor-made colloidal particles. *Curr. Opin. Colloid Interface Sci.* **2017**, *28*, 15–21. [CrossRef]
29. Porter, C.L.; Crocker, J.C. Directed assembly of particles using directional DNA interactions. *Curr. Opin. Colloid Interface Sci.* **2017**, *30*, 34–44. [CrossRef]
30. Buyong, M.R.; Kayani, A.A.; Hamzah, A.A.; Yeop, M.B. Dielectrophoresis Manipulation: Versatile Lateral and Vertical Mechanisms. *Biosensors* **2019**, *9*, 30. [CrossRef]
31. Miyagawa, A.; Okada, T. Particle Manipulation with External Field; From Recent Advancement to Perspectives. *Anal. Sci.* **2021**, *37*, 69–78. [CrossRef] [PubMed]
32. Zhao, W.; Brook, M.A.; Li, Y. Design of Gold Nanoparticle-Based Colorimetric Biosensing Assays. *ChemBioChem* **2008**, *9*, 2363–2371. [CrossRef]
33. Mannelli, I.; Marco, M.-P. Recent advances in analytical and bioanalysis applications of noble metal nanorods. *Anal. Bioanal. Chem.* **2010**, *398*, 2451–2469. [CrossRef]
34. Tauran, Y.; Brioude, A.; Coleman, A.W.; Rhimi, M.; Kim, B. Molecular recognition by gold, silver and copper nanoparticles. *World J. Biol. Chem.* **2013**, *4*, 35–63. [CrossRef]
35. Jazayeri, M.H.; Aghaie, T.; Avan, A.; Vatankhah, A.; Ghaffari, M.R.S. Colorimetric detection based on gold nano particles (GNPs): An easy, fast, inexpensive, low-cost and short time method in detection of analytes (protein, DNA, and ion). *Sens. Bio-Sens. Res.* **2018**, *20*, 1–8. [CrossRef]
36. Tang, Z.; Takarada, T.; Maeda, M. Non-Cross-Linking Aggregation of DNA-Carrying Polymer Micelles Triggered by Duplex Formation. *Langmuir* **2018**, *34*, 14899–14910. [CrossRef]
37. Zheng, Y.; Wang, Y.; Yang, X. Aptamer-based colorimetric biosensing of dopamine using unmodified gold nanoparticles. *Sens. Actuators B* **2011**, *156*, 95–99. [CrossRef]
38. Das, C.M.; Kong, K.V.; Yong, K.-T. Diagnostic plasmonic sensors: Opportunities and challenges. *Chem. Commun.* **2022**, *58*, 9573–9585. [CrossRef]
39. Zong, C.; Xu, M.; Xu, L.-J.; Wei, T.; Ma, X.; Zheng, X.-S.; Hu, R.; Ren, B. Surface-Enhanced Raman Spectroscopy for Bioanalysis: Reliability and Challenges. *Chem. Rev.* **2018**, *118*, 4946–4980. [CrossRef]
40. Bhaskar, S.; Moronshing, M.; Srinivasan, V.; Badiya, P.K.; Subramaniam, C.; Ramamurthy, S.S. Silver Soret Nanoparticles for Femtomolar Sensing of Glutathione in a Surface Plasmon-Coupled Emission Platform. *ACS Appl. Nano Mater.* **2020**, *3*, 4329–4341. [CrossRef]
41. Rai, A.; Bhaskar, S.; Genesh, K.M.; Ramamurthy, S.S. Engineering of coherent plasmon resonances from silver soret colloids, graphen oxide and Nd_2O_3 nanohybrid architectures studied in mobile phone-based surface plasmon-coupled emission platform. *Mater. Lett.* **2021**, *304*, 130632. [CrossRef]
42. Rai, A.; Bhaskar, S.; Genesh, K.M.; Ramamurthy, S.S. Hottest Hotspot from the coldest cold: Welcome to Nano 4.0. *ACS Appl. Nano Mater.* **2022**, *5*, 12245–12264. [CrossRef]
43. Jha, M.K.; Babu, B.; Parker, B.J.; Surendran, J.; Cameron, N.R.; Shaijumon, M.M.; Subramaniam, C. hierarchically Engineered Nanocarbon Florets as Bifunctional Electrode Materials for Adsorptive and Intercalative Energy Storage. *ACS Appl. Mater. Interfaces* **2020**, *12*, 42669–42677. [CrossRef]
44. Shi, L.; Liu, M.; Zhang, L.; Tian, Y. A Liquid Interfacial SERS Platform on a Nanoparticle Array Stabilized by Rigid Probes for the Quantification of Norepinephrine in Rat Brain Microdialysates. *Angew. Chem. Int. Ed.* **2022**, *61*, e202117125. [CrossRef]
45. Xu, L.-J.; Zong, C.; Zheng, X.-S.; Hu, P.; Feng, J.-M.; Ren, B. Label-free detection of native proteins by surface-enhanced Raman spectroscopy using iodide-modified nanoparticles. *Anal. Chem.* **2014**, *86*, 2238–2245. [CrossRef] [PubMed]
46. Fukunaga, Y.; Okada, T. Quantification using statistical parameters derived from signal intensity distributions in surface enhanced Raman scattering (SERS). *Anal. Chim. Acta* **2021**, *1181*, 338931. [CrossRef]
47. Fukunaga, Y.; Harada, M.; Okada, T. Surface-enhanced Raman scattering of DNA bases using frozen silver nanoparticle dispersion as a platform. *Microchim. Acta* **2021**, *188*, 406. [CrossRef]
48. Li, T.; Wu, X.; Liu, F.; Li, N. Analytical methods based on the light-scattering of plasmonic nanoparticles at the single particle level with dark-field microscopy imaging. *Analyst* **2017**, *142*, 248–256. [CrossRef]
49. Gao, P.F.; Lei, G.; Huang, C.Z. Dark-Field Microscopy: Recent Advances in Accurate Analysis and Emerging Applications. *Anal. Chem.* **2021**, *93*, 4707–4726. [CrossRef]
50. Li, M.-X.; Zhao, W.; Wang, H.; Li, X.-L.; Xu, C.-H.; Chen, H.-Y.; Xu, J.-J. Dynamic Single Molecular Rulers: Toward Quantitative Detection of MicroRNA-21 in Living Cells. *Anal. Chem.* **2018**, *90*, 14255–14259. [CrossRef]

51. Zhang, D.; Wang, K.; Wei, W.; Liu, S. Single-Particle Assay of Poly(ADP-ribose) Polymerase-1 Activity with Dark-Field Optical Microscopy. *ACS Sens.* **2020**, *5*, 1198–1206. [CrossRef] [PubMed]
52. Dillen, A.; Mohrbacher, A.; Lammertyn, J. A Versatile One-Step Competitive Fiber Optic Surface Plasmon Resonance Bioassay Enabled by DNA Nanotechnology. *ACS Sens.* **2021**, *6*, 3677–3684. [CrossRef] [PubMed]
53. Sun, M.; Lu, P.; Yu, C.; Feng, F.; Li, Q.; Zhan, J.; Xu, M.; Liu, Y.; Yao, L. Force-Coded Strategy for the Simultaneous Detection of Multiple Tumor-Related Proteins. *Anal. Chem.* **2022**, *94*, 8992–8998. [CrossRef] [PubMed]
54. Miyagawa, A.; Oshiyama, K.; Nagatomo, S.; Nakatani, K. Semi-quantification of the binding constant based on bond breaking in a combined acoustic-gravitational field. *Analyst* **2022**, *147*, 4735–4738. [CrossRef]
55. Miyagawa, A.; Oshiyama, K.; Nagatomo, S.; Nakatani, K. Zeptomole detection of DNA based on microparticle dissociation from a glass plate in a combined acoustic-gravitational field. *Talanta* **2022**, *238*, 123042. [CrossRef]
56. Ashkin, A. Acceleration and Trapping of Particles by Radiation Pressure. *Phys. Rev. Lett.* **1970**, *24*, 156–159. [CrossRef]
57. Laurell, T.; Petersson, F.; Nilsson, A. Chip integrated strategies for acoustic separation and manipulation of cells and particles. *Chem. Soc. Rev.* **2007**, *36*, 492–506. [CrossRef]
58. Petersson, F.; Åberg, L.; Swärd-Nilsson, A.-M.; Laurell, T. Free Flow Acoustophoresis Microfluidic-Based Mode of Particle and Cell Separation. *Anal. Chem.* **2007**, *79*, 5117–5123. [CrossRef]
59. Yavuz, C.T.; Prakash, A.; Mayo, J.T.; Colvin, V.L. Magnetic separations: From steel plants to biotechnology. *Chem. Eng. Sci.* **2009**, *64*, 2510–2521. [CrossRef]
60. Iranmanesh, M.; Hulliger, J. Magnetic separation: Its application in mining, waste purification, medicine, biochemistry and chemistry. *Chem. Soc. Rev.* **2017**, *46*, 5925–5934. [CrossRef]
61. Ge, S.; Whitesides, G.M. "Axial" Magnetic Levitation Using Ring Magnets Enables Simple Density-Based Analysis, Separation, and Manipulation. *Anal. Chem.* **2018**, *90*, 12239–12245. [CrossRef]
62. Nemiroski, A.; Kumar, A.A.; Soh, S.; Harburg, D.V.; Yu, H.-D.; Whitesides, G.M. High-Sensitivity Measurement of Density by Magnetic Levitation. *Anal. Chem.* **2016**, *88*, 2666–2674. [CrossRef]
63. Ge, S.; Semenov, S.N.; Nagarkar, A.A.; Milette, J.; Christodouleas, D.C.; Yuan, L.; Whitesides, G.M. Magnetic Levitation To Characterize the Kinetics of Free-Radical Polymerization. *J. Am. Chem. Soc.* **2017**, *139*, 18688–18697. [CrossRef] [PubMed]
64. Mirica, K.A.; Shevkoplyas, S.S.; Phillips, S.T.; Gupta, M.; Whitesides, G.M. Measuring Densities of Solids and Liquids Using Magnetic Levitation: Fundamentals. *J. Am. Chem. Soc.* **2009**, *131*, 10049–10058. [CrossRef] [PubMed]
65. Bwambok, D.K.; Thuo, M.M.; Atkinson, M.B.; Mirica, K.A.; Shapiro, N.D.; Whitesides, G.M. Paramagnetic ionic liquids for measurements of density using magnetic levitation. *Anal. Chem.* **2013**, *85*, 8442–8447. [CrossRef]
66. Ge, S.; Nemiroski, A.; Mirica, K.A.; Mace, C.R.; Hennek, J.W.; Kumar, A.A.; Whitesides, G.M. Magnetic Levitation in Chemistry, Materials Science, and Biochemistry. *Angew. Chem. Int. Ed.* **2020**, *59*, 17810–17855. [CrossRef]
67. Ozefe, F.; Yildiz, A.A. Smartphone-assisted Hepatitis C detection assay based on magnetic levitation. *Analyst* **2020**, *145*, 5816–5825. [CrossRef] [PubMed]
68. Yaman, S.; Tekin, H.C. Magnetic Susceptibility-Based Protein Detection Using Magnetic Levitation. *Anal. Chem.* **2020**, *92*, 12556–12563. [CrossRef]
69. Andersen, M.S.; Howard, E.; Lu, S.; Richard, M.; Gregory, M.; Ogembo, G.; Mazor, O.; Gorelik, P.; Shapiro, N.I.; Sharda, A.V.; et al. Detection of membrane-bound and soluble antigens by magnetic levitation. *Lab Chip* **2017**, *17*, 3462–3473. [CrossRef]
70. Miyagawa, A. *Acoustic Levitation-Based Trace-Level Biosensing: Design of Detection Systems and Applications to Real Samples*; Springer Singapore Pre Ltd.: Singapore, 2021. [CrossRef]
71. Miyagawa, A.; Okada, Y.; Okada, T. Aptamer-Based Sensing of Small Organic Molecules by Measuring Levitation Coordinate of Single Microsphere in Combined Acoustic-Gravitational Field. *ACS Omega* **2020**, *5*, 3542–3549. [CrossRef]
72. Miyagawa, A.; Harada, M.; Okada, T. Multiple MicroRNA Quantification Based on Acoustic Levitation of Single Microspheres after One-Pot Sandwich Interparticle Hybridizations. *Anal. Chem.* **2018**, *90*, 13729–13735. [CrossRef]
73. Miyagawa, A.; Harada, M.; Okada, T. Zeptomole Biosensing of DNA with Flexible Selectivity Based on Acoustic Levitation of a Single Microsphere Binding Gold Nanoparticles by Hybridization. *ACS Sens.* **2018**, *3*, 1870–1875. [CrossRef] [PubMed]
74. Miyagawa, A.; Harada, M.; Okada, T. Zeptomole Detection Scheme Based on Levitation Coordinate Measurements of a Single Microparticle in a Coupled Acoustic-Gravitational Field. *Anal. Chem.* **2018**, *90*, 2310–2316. [CrossRef] [PubMed]
75. Miyagawa, A.; Inoue, Y.; Harada, M.; Okada, T. Acoustic Sensing Based on Density Shift of Microspheres by Surface Binding of Gold Nanoparticles. *Anal. Sci.* **2017**, *33*, 939–944. [CrossRef] [PubMed]
76. Wang, H.; Lu, J. A Review on Particle Size Effect in Metal-Catalyzed Heterogeneous Reactions. *Chin. J. Chem.* **2020**, *38*, 1422–1444. [CrossRef]
77. Le Goff, G.C.; Srinivas, R.L.; Hill, W.A.; Doyle, P.S. Hydrogel microparticles for biosensing. *Eur. Polym. J.* **2015**, *72*, 386–412. [CrossRef]
78. Herrmann, A.; Haag, R.; Schedler, U. Hydrogels and Their Role in Biosensing Applications. *Adv. Healthc. Mater.* **2021**, *10*, 2100062. [CrossRef]
79. Ong, C.-B.; Annuar, M.S.M.A. Hydrogels Responsive Towards Important Biological-Based Stimuli. *Polym. Sci. B* **2022**, *64*, 271–286. [CrossRef]
80. Culver, H.R.; Clegg, J.R.; Peppas, N.A. Analyte-Responsive Hydrogels: Intelligent Materials for Biosensing and Drug Delivery. *Acc. Chem. Res.* **2017**, *50*, 170–178. [CrossRef]

81. Park, H.-I.; Park, S.-Y. Smart Fluorescent Hydrogel Glucose Biosensing Microdroplets with Dual-Mode Fluorescence Quenching and Size Reduction. *ACS Appl. Mater. Interfaces* **2018**, *10*, 30172–30179. [CrossRef]
82. Krisch, E.; Gyarmati, B.; Barczikai, D.; Lapeyre, V.; Szilágyi, B.Á.; Ravaine, V.; Szilágyi, A. Poly(aspartic acid) hydrogels showing reversible volume change upon redox stimulus. *Eur. Polym. J.* **2018**, *105*, 459–468. [CrossRef]
83. Shah, S.; Yu, C.-N.; Zheng, M.; Kim, H.; Eggleston, M.S. Microparticle-Based Biochemical Sensing Using Optical Coherence Tomography and Deep Learning. *ACS Nano* **2021**, *15*, 9764–9774. [CrossRef] [PubMed]
84. Mortelmans, T.; Kazazis, D.; Padeste, C.; Berger, P.; Li, X.; Ekinci, Y. Poly(methyl methacrylate)-Based Nanofluidic Device for Rapid and Multiplexed Serological Antibody Detection of SARS-CoV-2. *ACS Appl. Nano Mater.* **2022**, *5*, 517–526. [CrossRef]
85. He, H.; Nie, R.; Lu, P.; Peng, X.; Li, X.; Chen, Y. Low-Cost and Convenient Microchannel Resistance Biosensing Platform by Directly Translating Biorecognition into a Current Signal. *Anal. Chem.* **2021**, *93*, 15049–15057. [CrossRef]
86. Einstein, A. Über die von der molekularkinetischen Theorie der Wärme geforderte Bewegung von in ruhenden Flüssigkeiten suspendierten Teilchen. *Ann. Phys.* **1905**, *322*, 549–560. [CrossRef]
87. Clayton, K.N.; Berglund, G.D.; Linnes, J.C.; Kinzer-Ursem, T.L.; Wereley, S.T. DNA Microviscosity Characterization with Particle Diffusometry for Downstream DNA Detection Applications. *Anal. Chem.* **2017**, *89*, 13334–13341. [CrossRef] [PubMed]
88. Ma, H.; Wereley, S.T.; Linnes, J.C.; Kinzer-Ursem, T.L. Measurement of Protein-Protein Interaction Dynamics Using Microfluidics and Particle Diffusometry. *Anal. Chem.* **2022**, *94*, 15655–15662. [CrossRef]
89. Das, D.; Chen, W.-L.; Chuang, H.-S. Rapid and Sensitive Pathogen Detection by DNA Amplification Using Janus Particle-Enabled Rotational Diffusometry. *Anal. Chem.* **2021**, *93*, 13945–13951. [CrossRef]
90. Chen, W.-L.; Chuang, H.-S. Trace Biomolecule Detection with Functionalized Janus Particles by Rotational Diffusion. *Anal. Chem.* **2020**, *92*, 12996–13003. [CrossRef]
91. Lin, Y.-T.; Vermaas, R.; Yan, J.; de Jong, A.M.; Prins, M.W.J. Click-Coupling to Electrostatically Grafted Polymers Greatly Improves the Stability of a Continuous Monitoring Sensor with Single-Molecule Resolution. *ACS Sens.* **2021**, *6*, 1980–1986. [CrossRef]
92. Yan, J.; van Smeden, L.; Merkx, M.; Zijlstra, P.; Prins, M.W.J. Continuous Small-Molecule Monitoring with a Digital Single-Particle Switch. *ACS Sens.* **2020**, *5*, 1168–1176. [CrossRef] [PubMed]
93. van Dongen, J.E.; Spoelstra, L.R.; Berendsen, J.T.W.; Loessberg-Zahl, J.T.; Eijkel, J.C.T.; Segerink, L.I. A Multiplexable Plasmonic Hairpin-DNA Sensor Based On Target-specific Tether Dynamics. *ACS Sens.* **2021**, *6*, 4297–4303. [CrossRef] [PubMed]
94. Kremser, L.; Blaas, D.; Kenndler, E. Capillary electrophoresis of biological particles: Viruses, bacteria, and eukaryotic cells. *Electrophoresis* **2004**, *25*, 2282–2291. [CrossRef]
95. Østergaard, J.; Heegaard, N.H. Capillary electrophoresis frontal analysis: Principles and applications for the study of drug-plasma protein binding. *Electrophoresis* **2003**, *24*, 2903–2913. [CrossRef] [PubMed]
96. Ma, G.; Shan, X.; Wang, S.; Tao, N. Quantifying Ligand-Protein Binding Kinetics with Self-Assembled Nano-oscillators. *Anal. Chem.* **2019**, *91*, 14149–14156. [CrossRef]
97. Ma, G.; Wan, Z.; Zhu, H.; Tao, N. Roles of entropic and solvent damping forces in the dynamics of polymer tethered nanoparticles and implications for single molecule sensing. *Chem. Sci.* **2020**, *11*, 1283–1289. [CrossRef]
98. Zhou, X.-L.; Yang, Y.; Wang, S.; Liu, X.-W. Surface Plasmon Resonance Microscopy: From Single-Molecule Sensing to Single-Cell Imaging. *Angew. Chem. Int. Ed.* **2020**, *59*, 1776–1785. [CrossRef]
99. Zhang, P.; Ma, G.; Dong, W.; Wan, Z.; Wang, S.; Tao, N. Plasmonic scattering imaging of single proteins and binding kinetics. *Nat. Methods* **2020**, *17*, 1010–1017. [CrossRef]
100. Li, Z.; Huang, X.; Liu, H.; Luo, F.; Qiu, B.; Lin, Z.; Chen, H. Electrochemiluminescence Biosensor for Hyaluronidase Based on the Adjustable Electrostatic Interaction between the Surface-Charge-Controllable Nanoparticles and Negatively Charged Electrode. *ACS Sens.* **2022**, *7*, 2012–2019. [CrossRef]
101. Brown, M.A.; Bossa, G.V.; May, S. Emergence of a Stern Layer from the Incorporation of Hydration Interactions into the Gouy-Chapman Model of the Electrical Double Layer. *Langmuir* **2015**, *31*, 11477–11483. [CrossRef] [PubMed]
102. Yi, M.; Nymeyer, H.; Zhou, H.-X. Test of the Gouy-Chapman theory for a charged lipid membrane against explicit-solvent molecular dynamics simulations. *Phys. Rev. Lett.* **2008**, *101*, 038103. [CrossRef]
103. Hagiya, K.; Miyagawa, A.; Nagatomo, S.; Nakatani, K. Direct Quantification of Proteins Modified on a Polystyrene Microparticle Surface Based on zeta Potential Change. *Anal. Chem.* **2022**, *94*, 6304–6310. [CrossRef] [PubMed]
104. Bhaskar, S.; Kambhampati, N.A.V.; Ganesh, K.M.; Sharma, M.; Srinivasan, V.; Ramamurthy, S.S. Metal-Free Graphene Pxide-Based Tunable Soliton and Plasmon Engineering for Biosensing Applications. *ACS Appl. Mater. Interfaces* **2021**, *13*, 17046–17061. [CrossRef] [PubMed]
105. Venugopalan, P.; Kumar, S. Highly Sensitive Plasmonic Sensor with Au Bow Tie Nanoantennas on SiO_2 Nanopillar Arrays. *Chemosensors* **2023**, *11*, 121. [CrossRef]

106. Bhaskar, S.; Das, P.; Srinivasan, V.; Bhaktha, S.B.N.; Ramamurthy, S.S. Plasmonic-Silver Sorets and Dielectric Nd_2O_3 nanorods for Ultrasensitive Photonic Crystal-Coupled Emission. *Mater. Res. Bull.* **2022**, *145*, 111558. [CrossRef]
107. Bhaskar, S.; Srinivasan, V.; Ramamurthy, S.S. Nd_2O_3-Ag Nanostructures for Plasmonic Biosensing, Antimicrobial, and Anticancer Applications. *ACS Appl. Nano Mater.* **2023**, *6*, 1129–1145. [CrossRef]